Supplementary Material

S1 Materials

1,5-diphenylcarbazide ($C_{13}H_{14}H_4O$) and phosphoric acid (H_3PO_4, ≥ 85.0 wt%) were provided by YF Chemical Co., Ltd. (China). Urea (H_2NCONH_2), sodium hydroxide (NaOH), and potassium hydroxide (KOH) were sourced from Tianjin Fengchuan Chemical Reagent Technologies Co., Ltd. (China). Acetone (CH_3COCH_3) was obtained from Beijing Chemical Co., Ltd. (China). Hydrochloric acid (HCl, 36.0 wt%–38.0 wt%) and sulfuric acid (H_2SO_4, 98.0 wt%) were purchased from Luoyang Haohua Chemical Reagent Co., Ltd. (China). Potassium dichromate ($K_2Cr_2O_7$) were sourced from Tianjin Deen Chemical Reagent Co., Ltd. (China). The solutions were prepared with deionized water in the experiments. All the chemicals were used as received without any pre-treatment.

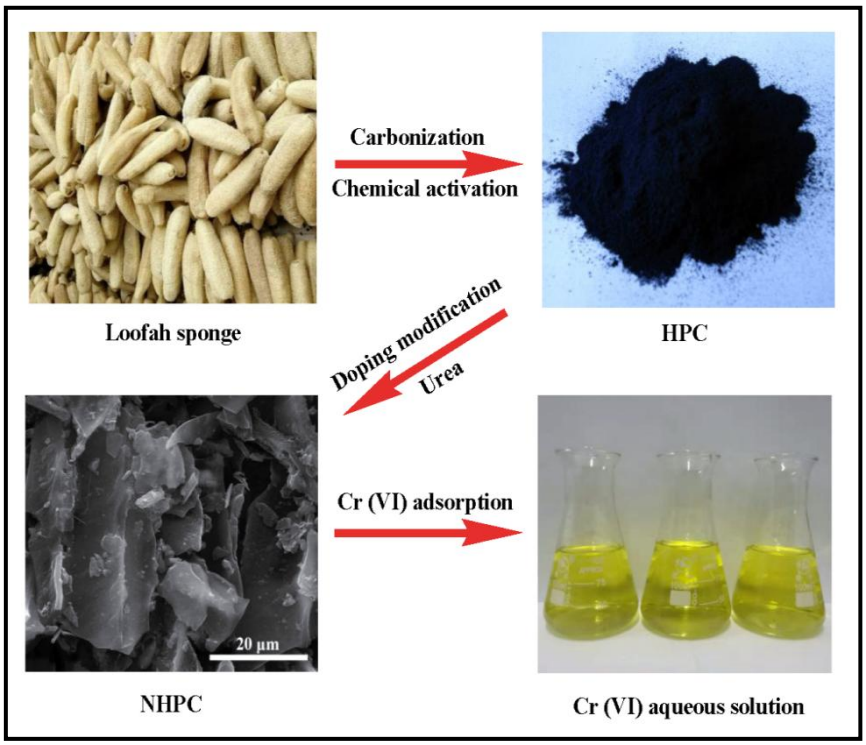

Fig. S1 Schematic illustration of the synthesis of NHPC

S2 Materials characterization

The microstructures of the adsorbents were characterized by a field-emission scanning electron microscopy (FESEM, JSM-6360LV, Japan) with an energy-dispersive spectrometer (EDS). The

crystalline structures were obtained through X-ray powder diffraction (XRD, Rigaku-TTRIII, Japan) analysis operating on a Cu-K_α radiation source (λ = 1.5406 Å) over a range of 10°–80 °. A Raman spectrometer (LabRAM Hr800, HORIBA Jobin Yvon, France) was used to record the Raman spectra with a wave number scope of 500–2500 cm^{-1}. The variations of the functional groups on the adsorbent surfaces were analyzed by Fourier transform infrared spectra (FTIR, Nicolet Nexus 470, USA). The specific surface area and pore volume of the as-prepared specimens were measured by Brunauer-Emmett-Teller (BET) method attained by a specific surface area and porosity analyzer (ASIQM 0010-4, Quantachrome, USA), and the nitrogen desorption isotherm was used to analyze the pore size distribution by the Barrett-Joyner-Halenda (BJH) method. The elemental valence states of the samples were analyzed using X-ray photoelectron spectroscopy (XPS, Thermo Kalpha, USA) with Al K radiation as the excitation source. The solution pH in the experiments was measured by the pH detector (PHS-3C, China). The relationship between pH and zeta potential was studied by a Malvern Zetasizer (Mastersizer 3000, Malvern, UK). A camera of smart phone (HUAWEI Nova 7 5G, China) was used to obtain the digital photographs.

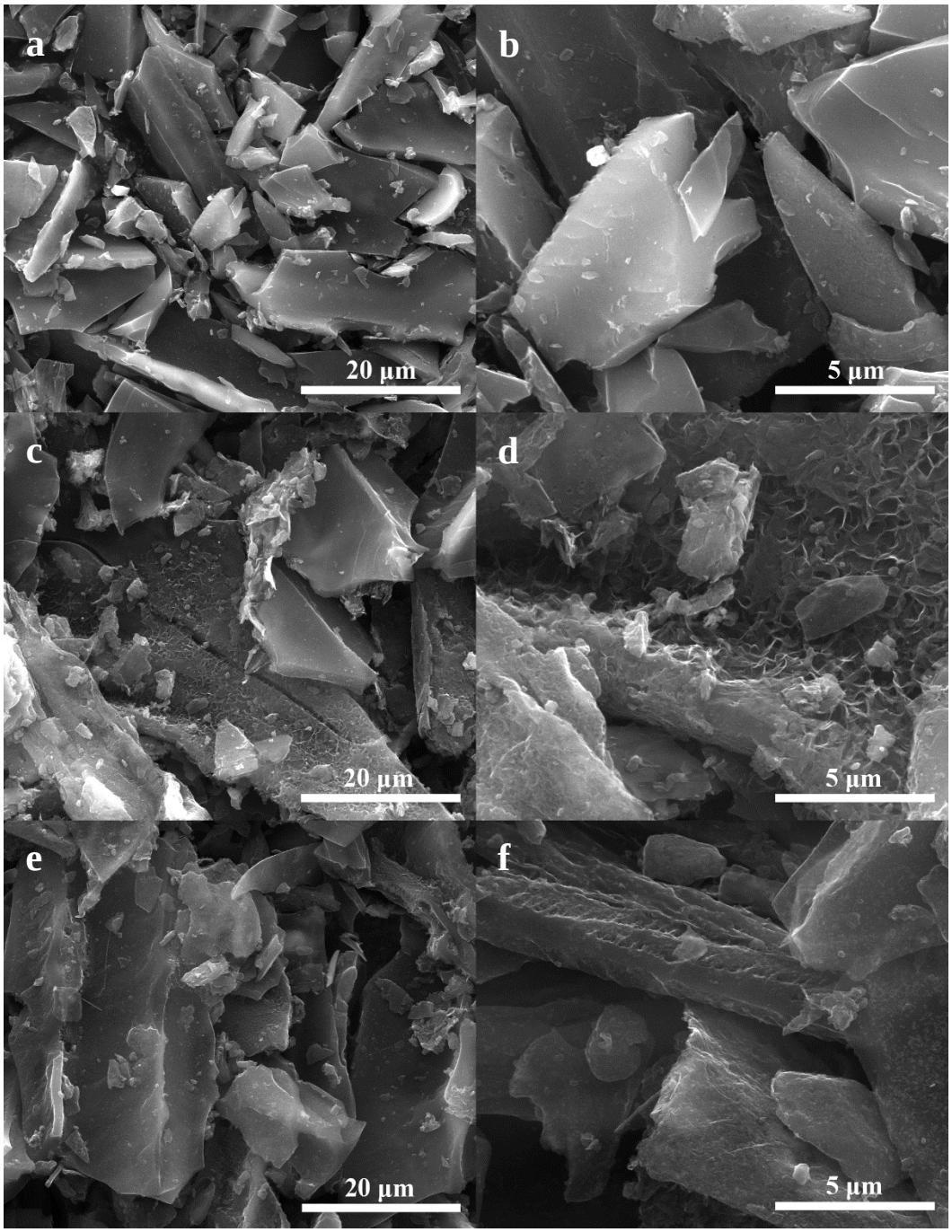

Fig. S2 SEM images of LSC (a, b), HPC (c, d), and NHPC (e, f)

S3 Comparison of adsorption characteristics

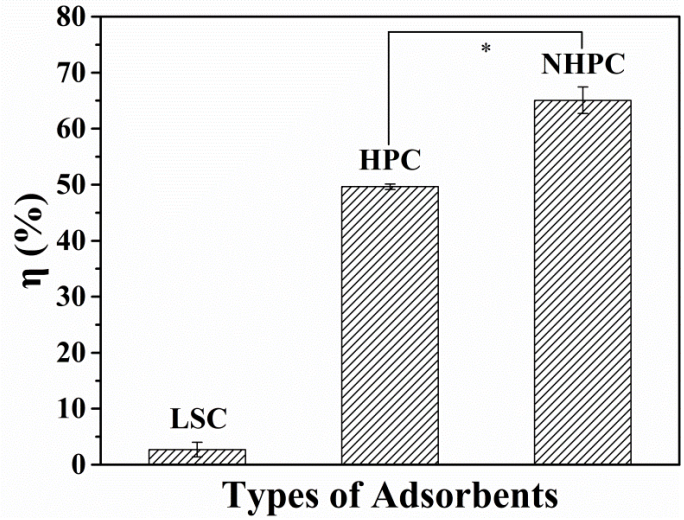

Fig. S3 Effect of different types of adsorbents on the adsorption efficiency of Cr (VI) under the same adsorption conditions (adsorbent: 1 g/L, pH = 5.6, initial Cr (VI) concentration = 10 mg/L, temperature = 298K, adsorption time = 24 h). * indicates significant differences ($p < 0.05$) between the two sets of data groups

S4 Zeta potential

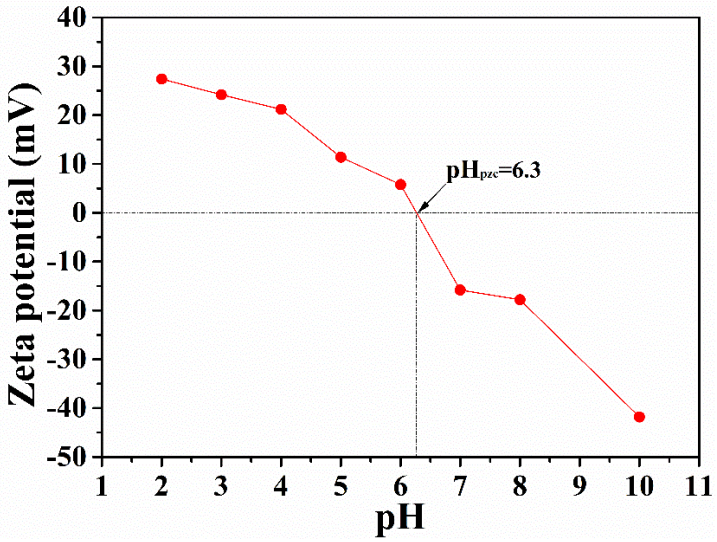

Fig. S4 The Zeta potential of NHPC

S5 Adsorption experiments and DFT calculation

To compare the adsorption efficiencies of Cr (VI) on the different types of adsorbents, 1 g/L of these three adsorbents, LSC, HPC, and NHPC, were separately added to the solution of 10 mg/L Cr (VI) for 24 h adsorption. The influence of pH on the Cr (VI) adsorption was researched by adjusting pH at 2, 3, 4, 6, 8, and 12 in the 10 mg/L Cr (VI) solution for 24 h at 298K, the dose of

NHPC was 0.1 g/L. The pH of Cr (VI) solutions was adjusted drop-wise by adding 0.1 mol/L NaOH or HCl. To study the influence of NHPC dose on the Cr (VI) adsorption, 0.06 to 0.14 g/L NHPC was applied to the 10 mg/L Cr (VI) solutions for 24 h at pH of 2 and 298K.

The kinetics adsorption experiments were implemented in a 100 mL Erlenmeyer flask, where 0.1 g/L of NHPC was added into the Cr (VI) solution (10 mg/L) in 50 mL with a pH of 2 at a broad temperature range (298K, 308K, and 318K). At disparate time intervals (1, 3, 5, 10, 20, 30, 60, 120, 240, 480, 720, 1080, and 1440 min), the mixtures were immediately filtered to determine the Cr (VI) concentrations in the filtrate. The pseudo-first-order and pseudo-second-order kinetic models were applied to fit the adsorption dynamics data, and the relevant equations were the following (Hussain et al., 2020).

Pseudo-first-order kinetics model:

$$\ln\left(q_e - q_t\right) = \ln q_e - k_1 t, \tag{S1}$$

Pseudo-second-order kinetics model:

$$\frac{t}{q_t} = \frac{1}{k_2 q_e^2} + \frac{t}{q_e}, \tag{S2}$$

where q_e (mg/g) and q_t (mg/g) indicated the quality of Cr (VI) adsorbed on the adsorbent at equilibrium time and at the given time t (min), respectively. k_1 (min^{-1}) and k_2 (g/(mg·min)) were the speed constants of the two kinetics models, respectively.

The adsorption isotherms were assessed by dispersing 0.1 g/L of NHPC with Cr (VI) solution at various initial concentrations (5, 10, 20, 30, 40, 50, 60, 70, and 90 mg/L) in the Erlenmeyer flasks. The pH of Cr (VI) solutions was adjusted to 2, and the flasks oscillated at different temperatures (298K, 308K, and 318K) for 480 min as described above. The Langmuir and Freundlich isotherm models were applied to fit the adsorption isotherm data as shown in the following equations (El Nemr et al., 2021; Sun et al., 2021).

Langmuir isotherm model:

$$\frac{C_e}{q_e} = \frac{1}{K_L q_m} + \frac{C_e}{q_m}, \tag{S3}$$

where C_e (mg/L) was the equilibrium concentration of Cr (VI) solution, K_L (L/mg) was a constant, and q_m (mg/g) represented the theoretical maximum adsorption capacity of adsorbent corresponding to complete monolayer coverage.

Further, the shape of the isotherm and the adsorption process was predicted by a dimensionless separation parameter (R_L), which indicated the nature of the adsorption and affected the shape of the adsorption curve. In general, the adsorption process could be evaluated to be irreversible (R_L = 0), favorable ($0<R_L<1$), linear (R_L = 1), or unfavorable ($R_L>1$) (Sun et al., 2021).

$$R_L = \frac{1}{1 + K_L C_0}, \tag{S4}$$

where C_0 (mg/L) was the highest initial concentration of Cr (VI).

$$\ln q_e = \ln K_F + \frac{1}{n} \ln C_e , \tag{S5}$$

where K_F (L/mg) was the Freundlich constant associated with the adsorption capacity of adsorbent and 1/n was the heterogeneity constant indicating how favorable the adsorption process was. For instance, the 1/n values were between 0 and 1, implying the favorable adsorption.

To explain the nature and spontaneity of adsorption process, the thermodynamic parameters, such as standard Gibbs free energy (ΔG°, kJ/mol), standard enthalpy change (ΔH°, kJ/mol), and standard entropy change (ΔS°, J/(mol·K)) were also calculated according to the isotherm data, the relevant equations were as follows (Fazlzadeh et al., 2017).

$$K_d = \frac{m q_e}{C_e V} , \tag{S6}$$

$$\ln K_d = \frac{\Delta S^o}{R} - \frac{\Delta H^o}{RT} , \tag{S7}$$

$$\Delta G^o = -RT \ln K_d , \tag{S8}$$

where K_d was the distribution coefficient, m (g) was the dosage of the adsorbent, and V (L) was the volume of the Cr (VI) solution.

To investigate the regeneration and reusability of the adsorbent, the adsorption-desorption experiments were carried out. Typically, 0.1 g/L of NHPC was added to 50 mL of the 90 mg/L Cr (VI) solution and oscillated on a thermostatic oscillator at 120 r/min for 480 min at 298K with the pH of Cr (VI) solutions adjusted to 2. After the adsorption, the NHPC-Cr was washed with deionized water and separated by filtration. The collected adsorbent was placed in an Erlenmeyer flask and immersed in 50 mL 0.5 mol/L NaOH solutions under stirring at 120 r/min for 240 min at 298K, followed by washing with deionized water until the pH reached 7 and drying at 378K in an oven. The regenerated adsorbent was directly used in the same adsorption tests with the Cr (VI) solutions. The adsorption efficiency and capacity were evaluated respectively.

The next-mentioned experiments were implemented with triplicate independent sampling or testing at least: 1) Cr (VI) batch adsorption experiments, 2) the concentration measurement of Cr (VI). All the experimental data were presented with mean values with standard deviation (less than 5%) as error bars. The standard curve of Cr (VI) was established with 9 concentration points (R^2 = 0.9995). The differences between experimental and control groups were tested for significance using the *t*-test at a significant level of 0.05.

The DFT calculation was carried out using version 3.0.3 of the ORCA quantum chemistry program package at the level of BLYP/def2-SVP (Ramirez et al., 2020). The computational accuracy of the noncovalent interaction in the def2-SVP basis group was optimized using the geometrical counterpoise (gCP) method. The dispersion calibration DFT-D3 was applied to describe the noncovalent interaction better (Huang and Hu, 2020). In the DFT calculation, various carbon adsorbents were extracted as the simplified models and then used as the initial structures

based on the outcomes of different detection analyses, and Cr (VI) primarily existed as the $HCrO_4^-$ at pH = 2. Hence, the adsorption energy (E_{ads}) of $HCrO_4^-$ on the carbon adsorbents was first calculated by the following equation (Wang et al., 2019; Huang and Hu, 2020).

$$E_{ads} = E(C\cdots HCrO_4^-) - E(C) - E(HCrO_4^-), \quad \text{(S9)}$$

where $E(C\cdots HCrO_4^-)$ referred to the total energy of $HCrO_4^-$ adsorbed on the surface of adsorbents, E(C) and $E(HCrO_4^-)$ were taken as respectively the energies of the free carbon adsorbents and $HCrO_4^-$. Moreover, the noncovalent interactions between various adsorbents and $HCrO_4^-$ had also been quantified by Multiwfn (Liang et al., 2019). In addition, the adsorption energy (E_{ads}) of CrO_4^{2-} on the carbon adsorbents was also calculated according to the above method.

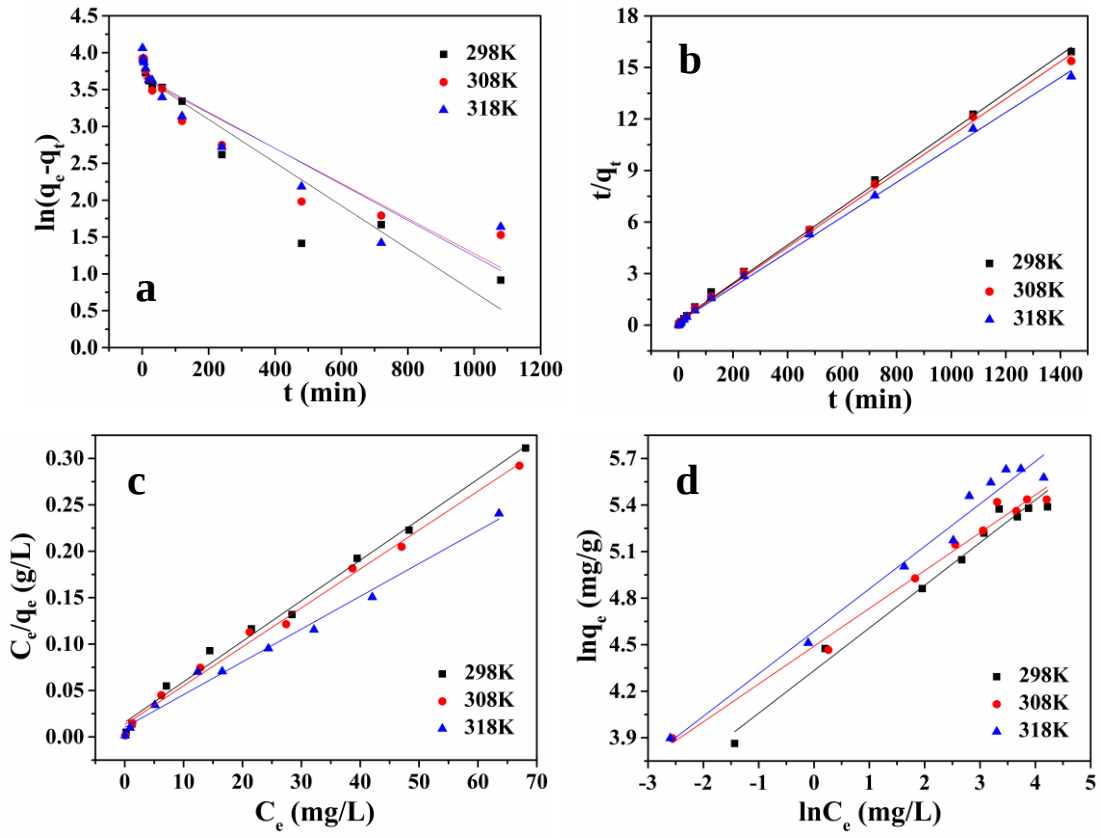

Fig. S5 (a) Pseudo-first-order kinetics model, (b) pseudo-second-order kinetics model, (c) Langmuir isotherm model, and (d) Freundlich isotherm model for Cr (VI) adsorption onto NHPC at various temperatures

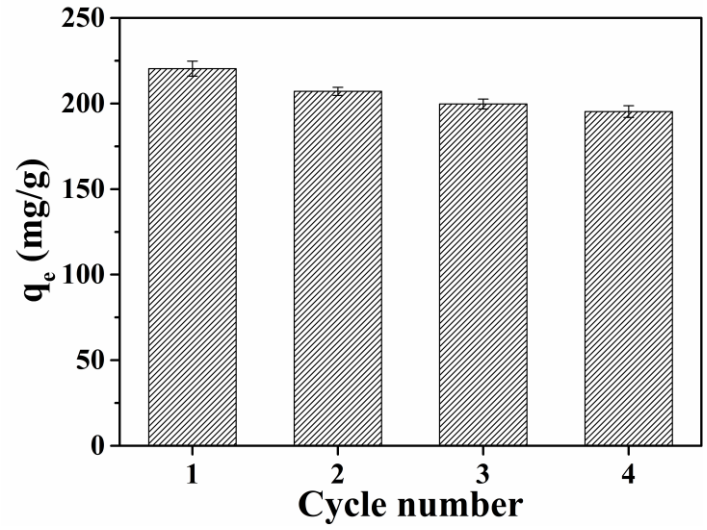

Fig. S6 The regeneration ability of NHPC for the adsorption of Cr (VI) over 4 cycles

Table S1 The adsorption kinetics and isotherm parameters of Cr (VI) by NHPC

Models	Parameters	Temperature (K)		
		298	308	318
Pseudo-first-order kinetics model	k_1 (min^{-1})	0.0029	0.0024	0.0024
	$q_{e, cal}$ (mg/g)	39.66	38.65	39.59
	$q_{e, exp}$ (mg/g)	90.45	93.65	99.51
	R^2	0.9068	0.8906	0.8710
Pseudo-second-order kinetics model	k_2 (g/(mg·min))	0.00048	0.00056	0.00061
	$q_{e, cal}$ (mg/g)	90.09	92.59	98.04
	$q_{e, exp}$ (mg/g)	90.45	93.65	99.51
	R^2	0.9985	0.9983	0.9985
Langmuir isotherm model	q_m (mg/g)	227.27	238.10	285.71
	K_L (L/mg)	0.28	0.32	0.34
	R^2	0.9926	0.9934	0.9874
	R_L	0.038	0.033	0.031
Freundlich isotherm model	K_F (L/mg)	76.19	89.16	98.14
	1/n	0.27	0.24	0.27
	R^2	0.9808	0.9861	0.9785

Table S2 The thermodynamic data of Cr (VI) by NHPC

Temperature (K)	ΔH° (kJ/mol)	ΔS° (J/(mol·K))	ΔG °(kJ/mol)	k_d
298	18.44	66.76	−1.49	1.82
308			−2.05	2.22
318			−2.83	2.92

S6 Analysis of the Cr (VI) adsorption mechanism

Table S3 Binding energies and relative contents of Cr, C, N, and O in NHPC and NHPC-Cr

Element	Assignments	NHPC		NHPC-Cr	
		Binding energy (eV)	Relative content (%)	Binding energy (eV)	Relative content (%)
Cr $2p_{1/2}$	Cr (VI)			588.3	13.72
	Cr (III)			586.8	20.02
Cr $2p_{3/2}$	Cr (VI)			578.5	22.02
	Cr (III)			577.4	44.24
C 1s	C-C/C-H	284.8	67.79	284.8	55.68
	C-OH	285.9	9.90	285.4	24.92
	C = O	286.9	6.59	287.1	12.45
	O-C = O	290.3	15.72	290.8	6.95
N 1s	-*N* =	398.6	14.43	398.6	7.58
	-NH-	399.8	50.31	400.0	41.69
	$-NH^+=$	400.9	19.84	401.0	31.24
	$-NH^+_2-$	402.8	15.42	402.5	19.49
O 1s		532.3		531.9	

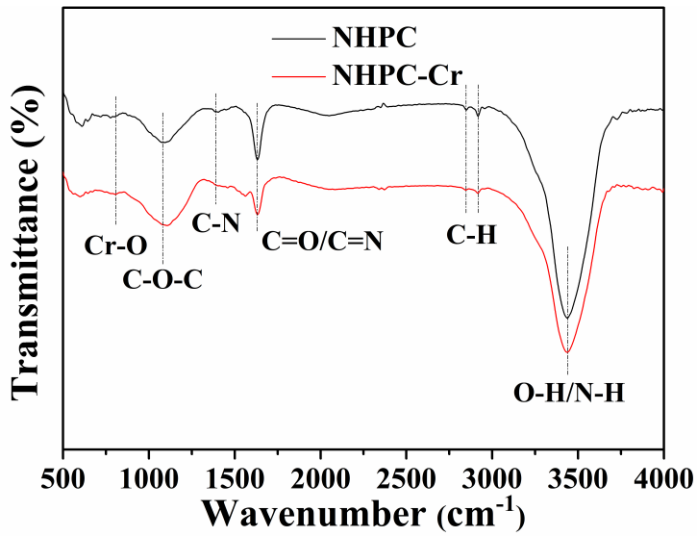

Fig. S7 FTIR spectra of NHPC and NHPC-Cr

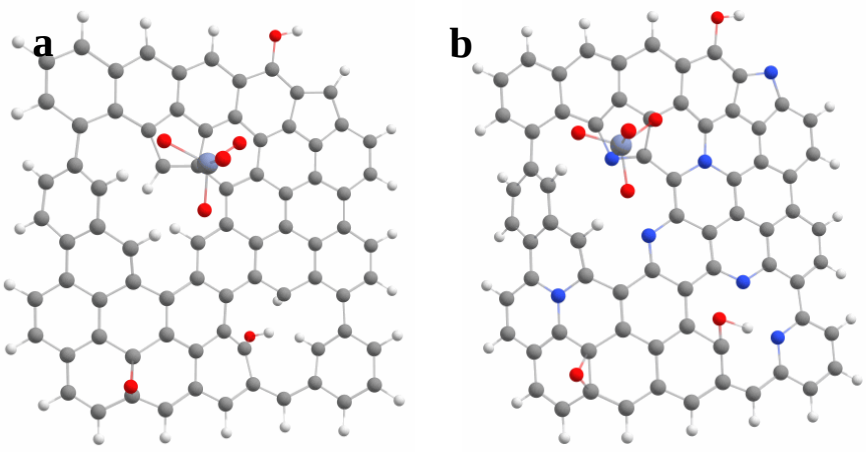

Fig. S8 The adsorption energies between the CrO_4^{2-} and absorbents ((a) HPC and (b) NHPC)

References

El Nemr A, Aboughaly R M, El Sikaily A, Ragab S, Masoud M S, Ramadan M S (2021). Utilization of sugarcane bagasse/ZnCl2 for sustainable production of microporous nano-activated carbons of type I for toxic Cr(VI) removal from aqueous environment. Biomass Conversion and Biorefinery, doi:10.1007/s13399-021-01445-6

Fazlzadeh M, Khosravi R, Zarei A (2017). Green synthesis of zinc oxide nanoparticles using Peganum harmala seed extract, and loaded on Peganum harmala seed powdered activated carbon as new adsorbent for removal of Cr(VI) from aqueous solution. Ecological Engineering, 103: 180–190 doi:10.1016/j.ecoleng.2017.02.052

Huang Y, Hu H (2020). The interaction of perrhenate and acidic/basic oxygen-containing groups on biochar surface: A DFT study. Chemical Engineering Journal, 381: 122647 doi:10.1016/j.cej.2019.122647

Hussain I, Qi J, Sun X, Wang L, Li J (2020). Melamine derived nitrogen-doped carbon sheet for the efficient removal of chromium (VI). Journal of Molecular Liquids, 318: 114052 doi:10.1016/j.molliq.2020.114052

Liang X, Fei Y, Xie Q, Liu Y, Lu M, Xia F, Nie Y, Ji J (2019). Sulfuryl fluoride absorption from fumigation exhaust gas by biobased solvents: thermodynamic and quantum chemical analysis. Industrial & Engineering Chemistry Research, 58(12): 5018–5029 doi:10.1021/acs.iecr.8b06112

Ramirez A, Ocampo R, Giraldo S, Padilla E, Flórez E, Acelas N (2020). Removal of Cr (VI) from an aqueous solution using an activated carbon obtained from teakwood sawdust: Kinetics, equilibrium, and density functional theory calculations. Journal of Environmental Chemical Engineering, 8(2): 103702 doi:10.1016/j.jece.2020.103702

Sun X, Peng Q, Wang Z, Li C, Huang Y (2021). N-doped porous carbon derived from Cr-tanned leather shaving wastes for synergetic adsorption of Cr(VI) from aqueous solution. Materials Letters, 284: 128815 doi:10.1016/j.matlet.2020.128815

Wang Y, Zhao W, Zheng W, Chen S, Zhao J (2019). Preparation of N-doped carbon nanosheets from sewage sludge for adsorption studies of Cr(VI) from aqueous solution. Nanomaterials (Basel, Switzerland), 9(2): 265 doi:10.3390/nano9020265 PMID:30781359